Light Emission of Flame-Generated TiO_2 Nanoparticles: Effect of IR Laser Irradiation

Silvana De Iuliis[1,*], Roberto Dondè[1], Igor Altman[2]

[1]CNR-ICMATE, Institute of Condensed Matter Chemistry and Technologies for Energy,

Via R. Cozzi 53, 20125 Milan, Italy

[2]Combustion Sciences and Propulsion Research Branch, Naval Air Warfare Center Weapons Division,

1 Administration Circle, China Lake, CA 93555, USA

[*]correspondence: silvana.deiuliis@cnr.it

Keywords: TiO_2 nanoparticles, flame spray pyrolysis, light emission, IR laser irradiation

Abstract

The aim of this work is the analysis of the evolution of titania nanoparticles based on their light emission spectra. Measurements are performed during the synthesis of the nanoparticles in a flame spray, which is irradiated by a pulsed IR laser. Due to the relatively high energy band gap of titania of about 3 eV, the observed substantial light absorption at the laser wavelength of 1.064 μm, i.e. within the region of titania transparency, makes our study novel and interesting.

Laser-induced light emission at different laser fluences is compared with spontaneous light emission from titania nanoparticles in flame. For signal processing, Wien plot is introduced to obtain the particle temperature. A peculiar feature of the temperature difference of the irradiated and non-irradiated particles versus laser fluence is obtained. Three well-defined regions of this fluence curve are observed and discussed. with a particular attention on the plateau-like behaviour at very low laser fluence, followed by a linear increase. An anomalously high titania absorption is inferred in the linear region.

The increase of the Urbach energy is speculated to account for the change in the optical properties of titania nanoparticles. It is related to structural defects, and, therefore, the presence of energy levels in the forbidden band due to the particular synthesis condition and/or induced by laser irradiation.

1. Introduction

Laser-induced incandescence (LII) is currently being considered a powerful diagnostic tool for the characterization of the condensed phase, in particular nano-sized and refractory particles, in combustion diagnostics of two-phase systems [1-4]. A pulsed laser rapidly heats a sample volume of nanoparticles, and their spectral incandescence radiation intensity is measured as the nanoparticles thermally equilibrate with the surrounding gas. We use the expression incandescence temperature for the temperature of the nanoparticles affected by laser irradiation.

It is well known that the peak of the incandescence signal is proportional to the particles concentration in the probe volume and it can be successfully employed in practical system with a proper calibration procedure [4-5]. Two-color laser-induced incandescence measurements are usually applied to derive incandescence temperature and particle concentration via a typical pyrometry approach [4-5]. Moreover, as small particles cool down faster than large particles, time-resolved LII measurements are currently carried out to infer the particle size from the emission decay after the laser pulse. This can be obtained by modelling the temperature decay curve with a consistent heat transfer mechanism. Recently, an interesting experimental approach has been applied to obtain spectrally and temporally resolved incandescence measurements combining a streak camera with a spectrometer [6, 7]

The LII has been widely employed in the characterization of combustion-generated carbon nanoparticles. In the recent years, the LII community has also become interested in application of the technique to synthetic nanoparticles, such as metallic [8, 9], metalloid [6, 7] and oxide nanoparticles [10, 11].

The characterization of these nanoparticles during and after the synthesis process [12, 13] can be of great importance for the fine synthesis control. Also the technique could be fruitfully applied in energetic combustion, in order to investigate the formation of oxide nanoparticles in metal-containing flames, since the energy released in the nanooxide growth accounts for more than 50% of total metal combustion enthalpy.

However, the application of the LII technique to synthetic particles is not straightforward. For example, for metal nanoparticles several unknown key points still remain to be explained [9]. In addition, these anomalies are also largely dependent on the particular material under analysis.

For example, an interesting evidence of enhanced absorption cross sections obtained comparing calorimetric and spectroscopic measurements has been detected in silver, molybdenum and iron nanoparticles. Although the application of Mie theory can in part explain these anomalies [9], problems remain to be solved and further work is needed to deeply understand the physics at the basis of these phenomena.

Concerning specifically the application of laser-induced incandescence to oxide nanoparticles, very few works are reported in the literature. In the work of Allen et al. [14] commercial alumina particles have been used and excited at room temperature by means of an IR laser pulse.

In our previous work, laser-induced incandescence measurements have been applied on titania nanoparticles produced via a hybrid burner [10], and after the applicability of the technique has been investigated on a flame spray. In this last work measurements have been performing under UV laser excitation [11]. However, being the excitation wavelength within the TiO_2 absorption band, an interference of the fluorescence band with incandescence occurs. For this reason, in order to discriminate incandescence from fluorescence, time-delayed incandescence measurements have been proposed 100 ns after the laser shot.

In the current work, we study the spectral behavior of light emission of TiO_2 nanoparticles irradiated by IR laser. Being the excitation wavelength significantly higher than the spectral region related to the typical absorption band (with an energy gap of about 3 eV), the occurrence of fluorescence can be avoided. Moreover, the irradiation with a low photon-energy IR laser allows to widen the dynamic range of energy excitation of the titania nanoparticles under analysis.

In this condition, the spectral feature of light emission is analyzed. To our knowledge, few works are reported in the literature concerning the TiO_2 IR excitation for LII measurements. In fact, in the work by Jafarkhani et al. [15] and Tian et al. [16], IR laser shot was essentially used for synthesis and not for diagnostic purpose. This can be probably due to the common understanding that oxides nanoparticles, being transparent in the visible range and near IR, might not absorb the laser energy required to induce a significant light emission.

Measurements are performed during the synthesis in a flame spray apparatus. In particular, laser-induced emission measurements versus wavelength are carried out varying the laser fluence. Signal is detected at a fixed height above the burner and at the peak of the laser shot. The direct comparison of the particle temperature under and without laser irradiation is performed in order to study the feature of the temperature-fluence curve during the synthesis in flame. Three well-defined regions of this fluence curve are observed. The change in the optical properties of titania nanoparticles is suggested as a way to reconcile the discussed issues including an anomalously high titania absorption inferred from the temperature-fluence curve.

The increase of the Urbach energy is speculated to account for the change in the optical properties of titania nanoparticles. It is related to structural defects, and, therefore, the presence of energy levels in the forbidden band due to the particular synthesis condition and/or induced by laser irradiation.

2. Theoretical approach

The radiation intensity I_p emitted at a wavelength λ by a cloud of nanoparticles is given by the following relationship:

$$I_P(T_P, fv) = A\, R_{BB}(T_P, \lambda)\, \epsilon(\lambda) \quad (1)$$

where R_{BB} is the energy spectral density and T_p the temperature of the heated particles, ε (λ) is the wavelength-dependent emissivity of the cloud of nanoparticles and A accounts for the probe volume. As shown in [17], we use the Wien function as R_{BB}, accounting for the emitting particles in a flame being in steady-state but not in equilibrium conditions. Based on the Kirchhof's law, the particle absorptivity is equal to its emissivity. Then, the spectral emissivity, $\varepsilon(\lambda)$, of nanoparticles can be expressed in terms of the emitting zone width, L, and absorption coefficient, K_{abs}, as follows

$$\varepsilon(\lambda) = 1 - exp\,(-K_{abs,\lambda}\, L) \quad (2)$$

which is, in turn, related to the particle volume fraction, f_V, as

$$K_{abs,\lambda} = \frac{36\,\pi\, fv}{\lambda} E(m) \quad (3)$$

In the previous relationship $E(m)$ is a function of the real and imaginary part of the refractive index, or in other words a function of the complex dielectric function of the particle material ε(λ)= ε′(λ) - i ε′′(λ)

$$E(m) = \frac{3\,\varepsilon''}{(\varepsilon'+2)^2+(\varepsilon'')^2} = \frac{6\,n\,k}{(n^2-k^2+2)^2+4\,n^2k^2} \quad (4)$$

being $\varepsilon' = n^2 - k^2$ and $\varepsilon'' = 2\,n\,k$.

In this work the emissivity in the 300 nm – 600 nm spectral range is obtained from absorption measurements on nanoparticles deposited on a glass plate [11]. We first use the same emissivity for each location in the flame, assuming that no changes in the nanoparticle optical properties occur along the flame. We discuss that the change in these properties is required in order to interpret our measurements. In situ measurements would be needed to directly demonstrate possible changes of the optical properties. However, such measurements are quite challenging and beyond the aim of the present work.

For the optically thin flame, $K_{abs,\lambda}L \ll 1$, and Eq. (1) can be re-written as

$$I_P(T_P, fv) = \frac{A'}{\lambda^5} f_V \frac{E(m)}{\lambda} \exp\left(-\frac{C_2}{\lambda T_p}\right) \quad (5)$$

Taking the logarithm of Eq. (5) we can derive the following expression

$$\ln(I_\lambda \lambda^5) = \ln(A') + \ln(f_V) - \frac{C_2}{\lambda T_p} + \ln[E(m)/\lambda] \quad (6)$$

where C_2 = 14388 μm K is the radiation constant, and A' accounts for the constant terms in the relationship. From the Wien plot, that is reporting $ln(I_\lambda * \lambda^5)$ vs wavenumber, a straight line is obtained if the absorption coefficient, that is $E(m) / \lambda$, is constant, and not wavelength dependent. The slope of the straight line, K, by definition gives the graybody temperature of the radiation, T^g

$$T^g = \frac{C_2}{K}, \quad (7)$$

an auxiliary value, which is convenient to use for further spectra processing in the real system with the wavelength-dependent absorption coefficient. It should be noted that the expression similar to Eq. (6) was used as a basis for the soot temperature inference in Ref. [18], but at the data processing $E(m)$ was taken to be constant.

Considering a wide gap semiconductor of a large disorder, as in the case of TiO_2 nanoparticles that have different defect energy states within the forbidden band, the Urbach law can describe the value q_{abs} as

$$q_{abs} \equiv \frac{E(m)}{\lambda} \propto B \exp\left(\frac{E}{E_U}\right) = B \exp\left(\frac{C_2}{\lambda(E_U/k_B)}\right) \quad (8)$$

where k_B is the Boltzmann constant. The Urbach energy, E_U, depends on the concentration of defects in the forbidden band and may be quite large for the titania particles generated in the flame. The defect concentration increase leads to the Urbach energy increase, so the spectral dependence of the absorption becomes weaker. At the same time the pre-factor B also increases as the defect concentration increases. The physical meaning of Eq. (8) is that with the defect concentration increase, the role of transitions into and from the forbidden band becomes more significant. As it is further shown, the exponential dependence of the RHS of Eq. (8) is important for the measurement interpretation.

Considering absorption measurements for titania particles deposited on the filter, the Urbach energy can be obtained from the slope of the logarithm of the absorption coefficient versus the incident photon energy [19, 20]. In our case, a value of 1.37 eV is derived. That high value looks consistent with a high number of defects related to the flame synthesis [21, 22]. Note that the defects appear as a result of the local charge imbalance [22].

Note that although it has not been discussed in literature, the soot absorption coefficient can be also well fitted to the Urbach law. The Urbach energy of about 1.45 eV describes the soot absorption calculated using the soot refractive index reported in [23]. From that point of view, a comprehensive study of the known soot refractive indices in their relation to the Urbach absorption law might be interesting. It then should be added that using the Urbach law is a convenient way to process measured light emission spectra. Using Eq. (8) for the fourth term in the RHS of Eq. (6), we can get

$$\ln(I_\lambda \lambda^5) = \ln(A'B) + \ln(f_V) - \frac{C_2}{\lambda T_p} + \frac{C_2}{\lambda (E_U/k_B)} \tag{9}$$

Then, taking into account the definition of the graybody temperature by Eq. (7) and equating slopes of both sides of Eq. (9) as functions of the reciprocal wavelength, we arrive at

$$-\frac{1}{T^g} = -\frac{1}{T_p} + \frac{1}{E_U/k_B} \tag{10}$$

And, finally the relation between the actual temperature of the emitting system, T_p, and its graybody value can be derived as [24]

$$T_p = \frac{T^g}{1 + k_B T^g / E_U} \tag{11}$$

where k_B is the Boltzmann constant. Then, once the Urbach energy is known, the actual particle temperature can be directly inferred from the graybody temperature, according to Eq. (11).

In order to investigate the effect of laser irradiation, a direct comparison of the light emission from flame and the light emission from the laser-irradiated flame can be also performed. To this purpose, the ratio of the emission intensity, I_λ^*, at a certain elevated temperature, T^*, to the emission intensity of the flame without heating, I_λ^0, is investigated as a function of the reciprocal wavelength, according to the following relationship [18, 19] that assumes no change in the particle volume fraction:

$$\ln\left(\frac{I_\lambda^*}{I_\lambda^0}\right) = \frac{C_2}{\lambda}\left(\frac{1}{T^0} - \frac{1}{T^*}\right) + \ln\left[\frac{(E(m)^*)}{(E(m))}\right] \quad (12)$$

where a direct difference of two Wien plots at the corresponding temperatures is obtained. The second term in the RHS of Eq. (12) accounts for a change in the optical properties. The slope of the modified Wien plot yields the change of the reciprocal temperature, which is useful when the temperature of the unheated system, T^0, is known and when temperature-relating changes in optical properties can be neglected. Moreover, this method, being based on the ratio of two signals, does not request calibration.

In the following we call Eq. (6) Wien Plot and Eq. (12) modified Wien plot.

It should be added that the system heating T^*-T^0 inferred from the modified Wien plot is not significantly sensitive to T^0, then even if the temperature of the unheated system is not exactly known, the system heating can be obtained.

3. Experimental set-up

The experimental setup employed for laser-induced emission measurements is shown in Fig. 1. The fundamental frequency beam (1064 nm, 5 Hz) of a pulsed Nd:YAG laser (Big Sky CFR 400) is used, whose top-hat laser intensity cross section ensures to obtain a uniform heating temperature of the particles in the probe volume. In particular, a portion of the laser beam is selected by means of a diaphragm (Ø = 4 mm) and sent into the flame by using an 1190 mm lens. The radiation emitted by the nanoparticles is collected and focused by a lens (focal lens f = 225 mm) on an optical fiber, connected to the entrance slit of a spectrograph (Shamrock 303i), which is coupled with an ICCD camera (iSTAR 334T, Andor Technology). Considering the 3 mm diameter of the optical fiber and the 1:1 magnification of the collection optics, a spatial resolution of the emission intensity measurements results to be 3 mm. Moreover, in order to remove the second order diffraction of the spectrometer, a high-pass filter (305 nm, HPF in the Fig. 1) is positioned in front of the optical fiber. The spectral emission is collected with a 150 grooves/mm grating, obtaining a 0.28 nm spectral resolution.

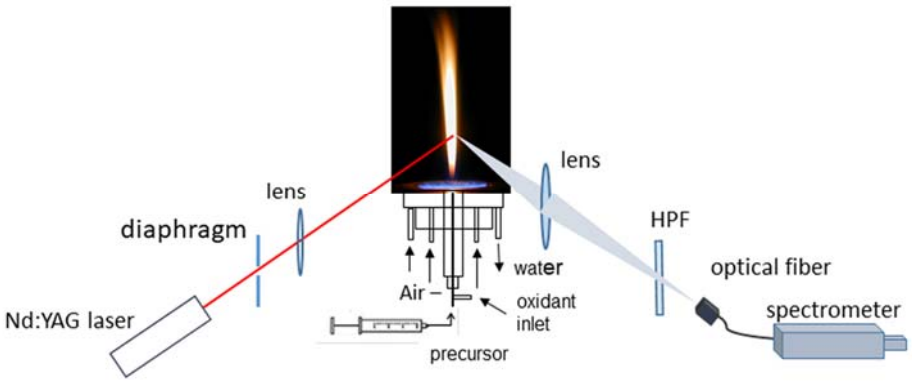

Fig. 1. Experimental set-up of laser-induced emission measurements in a flame spray apparatus. HPF is the high pass filter of 305 nm.

Measurements are performed on TiO_2 nanoparticles produced via a Flame Spray Pyrolysis (FSP) apparatus. A wide description of this apparatus is given in [11]; here only few details of the flame and of the experimental conditions under analysis are reported. FSP is essentially an oxygen-assisted spray apparatus, where the precursor is injected coaxially with the pilot fame. For the pilot flame, a water-coaled lamella burner is used to produce a sustaining methane/air lean premixed flame with an equivalence ratio of 0.8. The spray is obtained by means of a custom-made stainless steel gas-assisted spray injector consisting of a capillary inserted in the gas nozzle. The precursor solution flows through the capillary in a stream of O_2 used as nebulizing gas. The resulting droplets start to react with oxygen in a diffusion flame. By changing fuel and oxygen flow rates, the experimental conditions of the flame are changed (i.e. temperature field, gas velocity and consequently residence time as well as fuel/oxygen ratio).

Titanium tetraisopropoxide (Sigma-Aldrich, 97% purity, 3% isopropanol impurity) dissolved in ethanol (0.5 M) is used as a liquid precursor. The solution is injected at 4 ml/min feed rate through the spray nozzle by means of a syringe pump and nebulized by using a 5 Nl/min flow rate of O_2 stream. A synthesis diffusion flame of about 8 cm height is obtained, which is characterized by a very strong whitish emission due to a high flame temperature (about 2900 K, as measured in our previous work 11). TiO_2 nanoparticles are produced and collected on a glass fiber filter (150 mm diameter, Whatman Grade GF/A Glass Microfiber filter) downstream the reactor by a vacuum pump system for ex-situ measurements. In the above described conditions, the primary nanoparticle diameter is less than 20 nm as measured by STEM analysis.

In order to investigate the effect of the laser heating on titania nanoparticles, the spectral behavior of the laser-induced emission intensity is analyzed as a function of the laser energy density

(fluence) starting from very low values of the laser fluence. For these measurements, emission signal was collected at the peak of the laser with a gate width of 100 ns. In our previous work [11], as the 4th harmonic of the Nd:YAG laser (266 nm) was used, due to the fundamental absorption of TiO_2 nanoparticles, the interference of laser-induced emission with fluorescence had to be considered, as it may contaminate the incandescence signals. Due to the different characteristic lifetimes of the two phenomena, in order to neglect fluorescence, a 100 ns acquisition delay time with respect to the laser shot was chosen. In the present work, being IR laser excitation largely outside the titania absorption, any fluorescence emission can be neglected.

In all measurements, in order to check the effect of the laser irradiation and discriminate the laser-induced from the flame emission, signals are alternately collected with and without the laser, respectively, as described in [11]. Data are acquired by collecting 100 single shots. Because of tens of microseconds residence time of the titania nanoparticles in the probe volume and 5 Hz laser frequency used, a fresh probe volume was considered for each laser shot.

In order to confirm that the recorded light emission originates from the titania nanoparticles, the measurements were also repeated with the pure ethanol as a precursor. Under all conditions, the flame was bluish with no intensity change induced by the laser.

4. Results

As already reported in the experimental section, measurements have been alternately collected with and without the laser shot. Consequently, light emission from flame is also measured in each condition. As it will be discussed in the following, by fitting the Wien plot in the wavenumber range of its linearity, i.e., 1.7 – 2.6 μm^{-1}, the graybody temperature of the radiation T^g can be directly obtained from this slope. Moreover, according to Eq. (11) and considering the Urbach energy the temperature of particles present in the flame can be derived.

In Fig. 2 an example of the light emission from flame is shown and the corresponding Wien plot is also reported with the corresponding linear fitting. We note that light emission exhibits a typical continuous broad-band trend and the peak occurring at about 310 nm is due to OH* chemiluminescence emission. Note that this peak is not very pronounced in Fig. 2 due to the 305 nm filter used in the experiment.

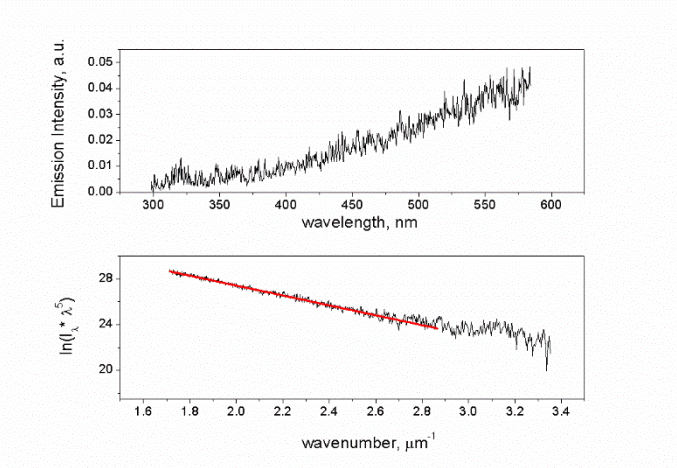

Fig. 2: Emission signal at HAB = 2 cm, corresponding Wien plot and fitting line to calculate the graybody temperature. The particle temperature is obtained considering the Urbach energy.

A value of the particle temperature of 2800 K is obtained at this HAB under analysis, with an uncertainty of about 1.36% evaluated taking into account the flame instability. This flame temperature is in agreement with the value derived in our previous work at the same height [11].

In Fig. 3 laser-induced light emission from titania nanoparticles versus wavelength, in the spectral range of 300 – 600 nm, is reported for the laser fluences under analysis. As it can be seen from the figure, increasing the laser fluence, the signal intensity increases as well.

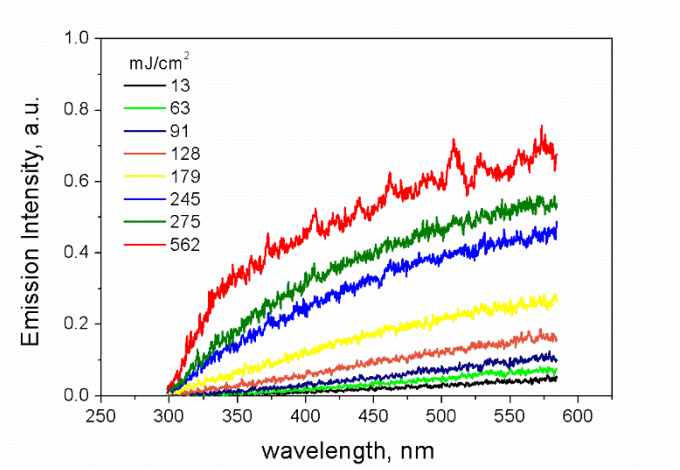

Fig. 3: Laser-induced light emission versus wavelength changing the laser fluence. Measurements performed at HAB = 2 cm.

At high laser fluence, significant peaks can be detected, probably due to photoluminescence of carbon-related molecules (such as C_2 Swan band). The identification of these species are beyond the aim of the present paper, and specific analysis including a mechanism of their excitation will be

performed in a future work. However, the presence of these photoluminescence bands overlapped on the continuous emission attributed to thermal radiation do not affect substantially the following processing procedure. In Fig. 4 the Wien plot, that is the $ln(I_\lambda \lambda^5)$ versus reciprocal wavelength, is reported for the fluences under study.

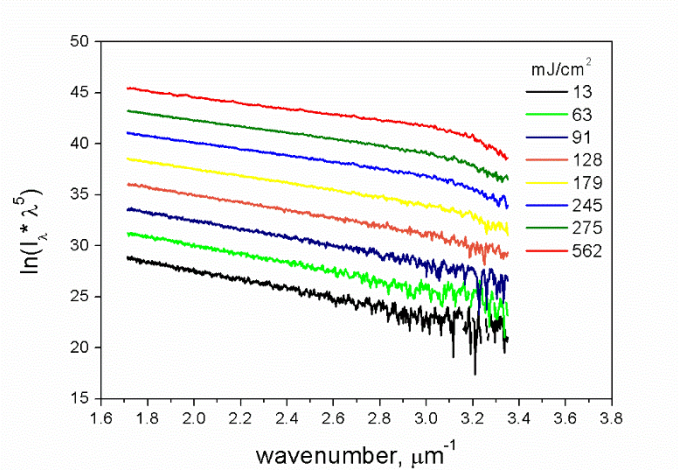

Fig. 4: Wien plot: $ln(I_\lambda \lambda^5)$ versus the reciprocal wavelength, changing the laser fluence. Measurements performed at HAB = 2 cm. The graphs are offset for an easier comparison

The signal exhibits a linear trend versus wavenumber ranging from 1.7 μm^{-1} up to about 2.6 μm^{-1}. Moreover, a significant drop in the signal is detected at higher wavenumber (μm^{-1}), that is more evident increasing the laser energy density and practically absent in the non-irradiated flame emission (see Fig. 2). This anomalous behavior occurs at the energy close/above to the optical band gap of about 3 eV of the titania synthesized in the flame, which is known from the literature [25, 26] and varies in the range of 3.0 - 3.2 eV for anatase and rutile. Since IR laser excitation is used in the present work, low energy photons are not enabled to excite electrons from the valence band to the conduction band. Correspondingly, the concentration of the conduction band electrons, which are responsible for a high energy emission is low. As a result, a different spectral behavior of particle emissivity at energies below and above the energy gap is possible, and a significant drop in the Wien plot of the laser-induced light emission is observed in the corresponding wavenumber region (>2.6 μm^{-1}).

By applying the same procedure already employed for the particle temperature in flame, the irradiated particle temperature is obtained using Eq. (11) with the Urbach energy of 1.37 eV measured for collected titania nanoparticles. The results are shown in Fig. 5 versus laser fluence.

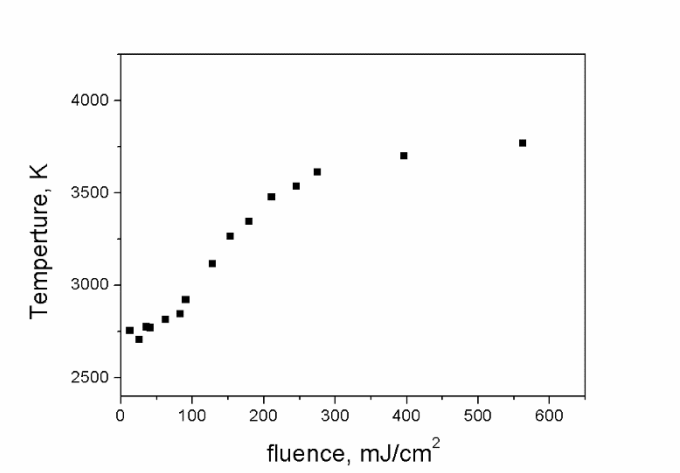

Fig. 5: Temperature of the irradiated particles versus the laser fluence obtained using Eq. (11) with the Urbach energy of 1.37 eV. HAB = 2 cm

Another way to look more carefully at this peculiar feature of the laser fluence curve is according to the modified Wien plot (Eq. (12)). In this way, the effect of laser irradiation on light emission from these particles can be directly highlighted. To this purpose, the ratio of the emission intensity from laser-irradiated flame and from flame is evaluated and the related logarithm reported versus the wavenumber. In Fig. 6 an example of the modified Wien plot, referring to a laser fluence of 275 mJ/cm^2, is shown.

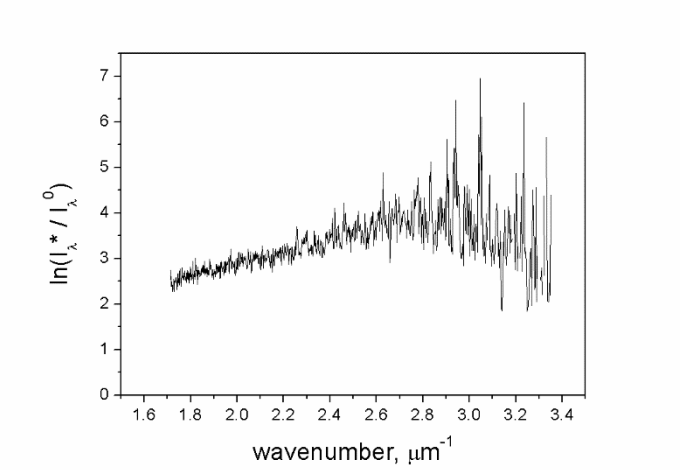

Fig. 6: Modified Wien plot: logarithm of the ratio of the laser-irradiated flame emission and flame emission versus wavenumber. Laser fluence of 275 mJ/cm^2

As it can be seen, a linear trend is shown for wavenumber up to about 2.6 μm^{-1}, followed by a sharp drop at higher wavenumber. The drop already mentioned above while discussing the Wien plot (Fig. 4) is the combined result of different effects of the optical band gap, which is more significant for the

laser-irradiated emission from particles than the corresponding emission from the not-irradiated particles. Although the logarithm of the ratio of the two signals is quite noisy, according to Eq. (12) and neglecting the possible change in the optical properties, the curve can be fitted with a straight line in the wavenumber range of 1.7 μm^{-1} – 2.6 μm^{-1}. From the slope of this fitting and assuming the value of the particle temperature in flame, the difference in the temperature of the particles affected and non-affected by laser irradiation can be obtained. In Fig. 7 this difference in particle temperature is reported versus laser fluence.

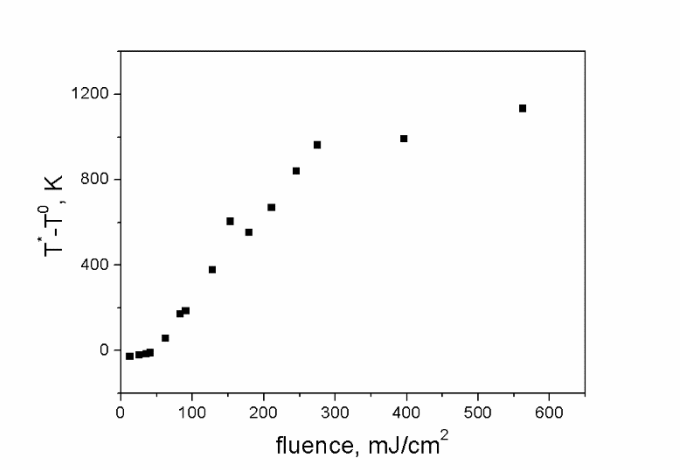

Fig. 7: Difference of particle temperature during laser irradiation and in flame versus laser fluence. HAB = 2 cm

From Figs. 5 and 7 it can be observed that increasing the laser fluence, three different regions can be distinguished. At very low laser fluence, up to 60 mJ/cm^2, a plateau-like region is observed. In the second region, this difference linearly increases with the fluence up to about 300 mJ/cm^2, above which a significant change in slope (but not flat behavior) is detected.

As it was already mentioned, the system heating inferred from the modified Wien plot is not significantly sensitive to the unheated system (non-irradiated flame) temperature. Then, regardless of the actual flame temperature, the system heating behavior preserves these major peculiarities seen in Fig. 7. It should be emphasized that Fig. 7, which describes the behavior of the temperature change with the laser fluence is obtained without using a particular value of the Urbach energy.

5. Discussion

In this section we discuss the peculiar features of the fluence curve reported in Fig. 5 for the particle temperature and in Fig. 7 for the difference in the particle temperature of the irradiated and not irradiated particles. As we have already underlined, three different regions can be detected in these curves. The first is the plateau-like region observed in the low laser fluence regime. To our

knowledge, it is the first time that such a plateau behavior has been detected at low laser fluence. Actually, by starting heating nanoparticles at very low fluence, one could expect to detect emission signal from these nanoparticles, related to an increase of the particle temperature, higher than the emission from not irradiated nanoparticles. Moreover, the difference in the temperature of irradiated and not-irradiated particles should increase with the fluence. This is in contrast from what we observe in our measurements. Although under laser irradiation, a considerable change in the light emission is observed at very low laser fluence, no change in its spectral behavior, and, correspondingly, in the temperature was detected. At higher laser fluence, above 60 mJ/cm^2, after a sharp knee a second region characterized by a linear increase of the temperature difference versus the laser fluence is detected (Fig. 7). This behavior is in agreement with typical fluence curves obtained in soot measurements. In fact, it is well known that at relatively low laser fluence the incandescence temperature of the particles under laser irradiation is related to the particle temperature in flame according to the following relationship [3]:

$$T^* - T^0 = \frac{6\,\pi\,E(m)\,F}{\lambda_{exc}\,c_p\rho_p} \qquad (13)$$

where $E(m)$ depends on the optical properties of the particles under analysis, c_p is the heat capacity, ρ_p the particle density, and λ_{exc} is the excitation wavelength. The difference in particle temperature linearly depends on the laser fluence F, and the slope of such dependence is strictly related to the optical properties. We note that, although Eq. (13) well describe the difference in temperature behaviour with the fluence in the second region, that is the linear trend in Fig. 7, it hardly can justify the plateau-like trend in the first region.

Moreover, considering Eq. (13) one should obtain the value of the flame temperature in correspondence of a 0 value of the laser fluence. On the contrary, in Fig. 7 the intercept of the linear fitting detected in the second region is a negative value: that means that a different temperature of the not irradiated particles is obtained.

A possible explanation of the plateau-like behavior is that this is just an apparent plateau, and the actual particle temperature does increase with the laser fluence. It might be possible if the Urbach energy changes with the laser fluence. Indeed, based on Eq. (11), at the same graybody temperature the Urbach parameter increase leads to the increase of the particle temperature. An explanation might be as that the laser irradiation affects the titania nanoparticles further enhancing the disorder, and, therefore, increasing the Urbach parameter. Then, the graybody temperature correction by Eq. (11) should be done accounting for that Urbach energy dependence on the laser fluence, which would lead

to the monotonously increasing resulting temperature dependence on the fluence and reconcile the plateau-relating feature.

Considering Eq. (13) in the medium fluence range, the value of E(m) can be estimated for the excitation wavelength of 1064 nm. In our case, by using a heat capacity of about 100 J/(mol K) [27], a value of 0.12 is derived for E(m). At the real part of the refractive index of 2.6, which is the value at the room temperature, the inferred E(m) corresponds to the imaginary part of the refractive index of 0.62. Assuming a possible decrease of the real part of the refractive index at the temperature of the experiment, the imaginary part of the refractive index is still high. For example at the real part of 2 the imaginary part of 0.37 is required to get E(m) = 0.12. The significant value of the imaginary part of the refractive index, related to the absorption properties of the nanoparticles, accounts for an important change in the optical properties of the particles under laser irradiation. Interestingly, the imaginary part of the titania refractive index is comparable to that of soot. This high value can be interpreted as a high conductivity of the titania nanoparticles under these conditions, which is a consequence of laser irradiation. In brief, the increase of the disorder occurring at low fluence becomes so large, that the concept of the energy gap is no more valid, which can potentially lead to the metal-like electrical conductivity. Then, at the energy gap shrinkage, the high conductivity is possible that explains the high imaginary part of the refractive index of the titania nanoparticles.

Considering again the second region of the fluence curve, we can observe that the value of the temperature difference in this region in Fig. 7 is about 1000 K. This means that the particle temperature in flame under laser irradiation can reach about 3800 K, well above the titania boiling point. Moreover, this value should be even higher if one take into account the change in the optical properties (increase in the Urbach energy with the disorder enhanced by the laser irradiation) previously discussed that would lead to some monotonous temperature increase in the first laser fluence region. This observation opens new questions to be solved, for example on the meaning of the temperature measured or on the modeling used to describe the phenomena involved.

The third region of the fluence curve (Fig. 5 and 7) is the section usually called “saturation”. Here, increasing the laser fluence above the linear part, a bending of the flame temperature is detected, even if not a real plateau is reached, at least in the fluence range investigated. As one can understand, the temperature observed in this region is well above the value of 3800 K discussed for the second region. More work is required to understand and interpret the dependence of temperature of titania nanoparticles on the laser fluence.

6. Conclusions

In this work we study the effect of IR laser irradiation on titania nanoparticles during the synthesis in a flame spray. Although titania nanoparticles are characterised by a relatively high-energy band gap (3 eV), they are found to absorb in the IR excitation region. It is ascribed to the presence of defects in the forbidden band due to the particular synthesis under analysis. Laser-induced emission from titania nanoparticles are detected and compared with the emission from not-irradiated nanoparticles in flame and the particle temperature dependence on the laser fluence is obtained. Some peculiar features are shown by this fluence curve. In particular, at very low laser fluence (below 60 mJ/cm^2) a plateau-like behaviour is observed up to a very sharp knee, above which the typical linear trend is obtained. In the saturation regime, we observe the bending of the flame temperature, even if a real plateau is not reached at least in the fluence range under analysis (up to about to 600 mJ/cm2).

The low fluence apparent temperature plateau is interpreted as a consequence of the changes of the optical properties of the nanoparticles because being a constant temperature for an increasing energy input a not physical behavior.

From the behaviour of the fluence curve in the low/medium fluence range the refractive index of titania nanoparticle is inferred. An extremely high imaginary part of the refractive index is obtained that is again attributed to a significant effect of laser irradiation on the optical properties.

In other words, laser irradiation can strongly change the inner structure of the nanoparticles, affecting the structural disorder dependent Urbach energy and consequently the absorption efficiency of these nanoparticles.

Acknowledgements

The work is supported by I-ZEB Project (Towards Intelligent Buildings Energy Zero for the Smart City Growth) in the framework of Lombardia Region – CNR agreement. I.A. thanks funding from the NAVAIR ILIR program managed at the ONR and administered by Alan Van Nevel.

Reference

1. Michelsen HA, Schulz C, Smallwood GJ, Will S. Laser-induced incandescence: Particulate diagnostics for combustion, atmospheric, and industrial applications. Prog Energy Comb Sci 2015;51:2-48. doi.org/10.1016/j.pecs.2015.07.001.
2. Migliorini F, De Iuliis S, Maffi S, Zizak G. Environmental application of pulsed laser-induced incandescence. Appl Phys B 2013;112:433-440. doi.org/10.1007/s00340-013-5385-6.
3. De Iuliis S, Migliorini F, Cignoli F, Zizak G. Peak soot temperature in laser-induced incandescence measurements. Appl Phys B 2006;83:397-402.
4. De Iuliis S, Cignoli F, Zizak G. Two-color laser-induced incandescence (2C-LII) technique for absolute soot volume fraction measurements in flames. Appl Opt 2005;44:7414-7423. doi.org/10.1364/ao.44.007414..
5. Snelling DR, Smallwood GJ, Liu F, Gulder OL, Bachalo WD. A calibration-independent laser-induced incandescence technique for soot measurement by detecting absolute light intensity. Appl Opt 2005;44(31):6773-6785. https://doi.org/10.1364/AO.44.006773.
6. Menser J, Daun K, Dreier T, Schultz C. Laser-induced incandescence from laser-heated silicon nanoparticles. Appl Phys B 2016;122:277. Doi.org/10.1007/s00340-016-6551-4.
7. Menser J, Daun K, Dreier T, Schultz C, Laser-induced atomic emission of silicon nanoparticles during laser-induced heating. Appl Opt 2017;56(11):E50. https://doi.org/10.1364/AO.56.000E50.
8. Sipkens TA, Singh NR, Daun KJ. Time-resolved laser-induced incandescence characterization of metal nanoparticles. Appl Phys B 2017;123(1):14. doi.org/10.1007/s00340-016-6593-7.
9. Talebi-Moghaddam S, Sipkens TA, Daun KJ. Laser-induced incandescence on metal nanoparticles: validity of the Rayleigh approximation. Appl Phys B 2019;125:214.
10. Maffi S, Cignoli F, Bellomunno C, De Iuliis S, Zizak G. Spectral effects in laser induced incandescence application to flame-made titania nanoparticles. Spectrochim Acta B 2008;63(2):202-209. doi.org/10.1016/j.sab.2007.11.022.
11. De Iuliis S, Migliorini F, Donde R. Laser-induced emission of TiO_2 nanoparticles in flame spray synthesis. Appl Phys B 2019;125(11):219 (2019). doi.org/10.1007/s00340-019-7324-7.
12. Liu C, Camacho J, Wang H. Phase Equilibrium of TiO_2 Nanocrystals in Flame-Assisted Chemical Vapor Deposition. Chem Phys Chem 2018;19:180-186. doi.org/10.1002/cphc.201700962.

13. Li S, Ren Y, Biswas P, Tse SD. Flame aerosol synthesis of nanostructured materials and functional devices: Processing, modeling, and diagnostics. Progr Energy Comb Sci 2016;55:1. doi.org/10.1016/j.pecs.2016.04.002.
14. Allen D, Krier H, Glumac N. Nano-Alumina Accommodation Coefficient Measurement Using Time-Resolved Laser-Induced Incandescence. J Heat Transf 2016;138:112401. https://doi.org/10.1115/1.4033642.
15. Jafarkhani P, Dadras S, Torkamany MJ, Sabbaghzadeh J. Synthesis of nanocrystalline titania in pure water by pulsed Nd: YAG Laser. Appl surf sci 2010;256(12):3817-3821. https://doi.org/10.1016/j.apsusc.2010.01.032.
16. Tian F, Sun J, Yang J, Wu P, Wang HL, Du XW. Preparation and photocatalytic properties of mixed-phase titania nanospheres by laser ablation. Mater Lett 2009;63(27):2384-2386. doi:10.1016/j.matlet.2009.08.018.
17. Altman IS. On principle inadequacy of the Plank distribution to the spectrum of the small particle thermal radiation. Phys Lett A 1999;256(2-3):122-124. doi.org/10.1016/S0375-9601(99)00222-4.
18. Snelling DR, Thomson KA, Smallwood GJ, Gülder Ö, Weckman EJ, Fraser RA. Spectrally resolved measurements of flame radiation to determine soot temperature and concentration. AIAA Journal 2002:40(9):1789-1795. doi.org/10.2514/2.1855.
19. Altman IS, Lee D, Song J, Choi M. Experimental estimate of energy accommodation coefficient at high temperatures. Phys Rev E 2001;64:052202. doi.org/10.1103/PhysRevE.64.052202.
20. Altman IS, Lee D, Chung JD, Song J, Choi M. Light absorption of silica nanoparticles. Phys Rev B 2001;63:161402. doi.org/10.1103/PhysRevB.63.161402.
21. Altman IS, Pikhitsa PV, Choi M. Key Effects in Nanoparticle Formation by Combustion Techniques. in Gas Phase Nanoparticle Synthesis, Edited by C.G. Granqvist, L.B. Kish, W.H. Marlow (Kluwer, Dordrecht, 2004) 43-67.
22. Jayashree S, Ashokkumar M. Switchable Intrinsic Defect Chemistry of Titania for Catalytic Applications. Catalysts 2018;8:601. doi.org/10.3390/catal8120601.
23. Chang H, Charalampopoulos T. Determination of the Wavelength Dependence of Refractive Indices of Flame Soot. Proceedings of The Royal Society A 1990;430(1880):577-591. DOI: 10.1098/rspa.1990.0107.
24. Altman IS. Determination of Particle Temperature from Emission Spectra. Combust Explo Shock 2004;40:67-69. doi.org/10.1023/B:CESW.0000013668.18664.ed.

25. Zhang J, Zhou P, Liu J, Yu J. New understanding of the difference of photocatalytic activity among anatase, rutile and brookite TiO_2. Phys Chem Chem Phys 2014;16:20382. https://doi.org/10.1039/C4CP02201G.
26. Studenyak I, Kranjcec M, Kurik M. Urbach Rule in Solid State Physics. International Journal of Optics and Applications 2014;4(3):76-83. doi: 10.5923/j.optics.20140403.02.
27. Linstrom PJ, Mallard WG, Eds., NIST Chemistry WebBook, NIST Standard Reference Database Number 69, National Institute of Standards and Technology, Gaithersburg MD, 20899, https://doi.org/10.18434/T4D303, (retrieved June 2, 2020).